Inorg. Chem. **2007**, *46*, 3645–3656

The First Ruthenium-Based Paullones: Syntheses, X-ray Diffraction Structures, and Spectroscopic and Antiproliferative Properties in Vitro

Wolfgang F. Schmid,[†] Stefanie Zorbas-Seifried,[‡] Roland O. John,[†] Vladimir B. Arion,*[,†] Michael A. Jakupec,[†] Alexander Roller,[†] Markus Galanski,[†] Ion Chiorescu,[†] Haralabos Zorbas,[‡] and Bernhard K. Keppler*[,†]

Institute of Inorganic Chemistry, Währingerstr. 42, A-1090 Vienna, Austria, and Max-Planck-Institute of Biochemistry, Am Klopferspitz 18, D-82152 Martinsried, Germany

Received January 19, 2007

Two novel paullone derivatives, namely, 6-(α-picolylamino)-7,12-dihydroindolo[3,2-*d*][1]benzazepine (**L^1**) and 9-bromo-6-(α-picolylamino)-7,12-dihydroindolo[3,2-*d*][1]benzazepine (**L^2**), have been prepared. The reaction of *cis*-[$RuCl_2(DMSO)_4$] (DMSO = dimethyl sulfoxide) with **L^1** and **L^2** in a 1:1 molar ratio in dry ethanol at 50 °C afforded the complexes *trans*-[$Ru^{II}Cl_2(DMSO)_2$**L^1**] (**1a**) and *trans*-[$Ru^{II}Cl_2(DMSO)_2$**L^2**] (**1b**) in 26 and 30% yield, respectively. The reaction carried out from the same starting compounds in a 1:2 molar ratio at 75 °C led to the formation of [$Ru^{II}Cl(DMSO)$(**L^1**)$_2$]Cl (**2a**) and [$Ru^{II}Cl(DMSO)$(**L^2**)$_2$]Cl (**2b**) in 16 and 23% yield, correspondingly. The products were characterized by elemental analysis, one- and two-dimensional NMR spectroscopy, electrospray ionization mass spectrometry, IR spectroscopy, electronic spectra, cyclic voltammetry, and X-ray crystallography (**L^1**, **L^2**, **1a**, and **2b**). Complexes **2a** and **2b** exhibit remarkable antiproliferative activity in three human carcinoma cell lines, A549 (non-small cell lung carcinoma), CH1 (ovarian carcinoma), and SW480 (colon carcinoma). The novel complexes show an intercalative mode of interaction with DNA, which may render them attractive alternatives to metal compounds with a coordinative mode of interaction.

Introduction

Metal complexes with biologically active ligands are a challenging subject of current research efforts.[1−3] Favorable effects upon complexation include (i) the stabilization of certain, sometimes unusual ligand geometries, (ii) acquired redox activity, (iii) increased solubility, (iv) enhanced cellular uptake, (v) different modes of action, and (vi) synergistic effects from metal and ligand(s).[4−12] Being involved in the development of metal-based antitumor drugs,[13−15] we focused our attention on the synthesis of metal complexes with ligands which exhibit high antiproliferative activity in vitro.

* To whom correspondence should be addressed. E-mail: vladimir.arion@univie.ac.at (V.B.A.), bernhard.keppler@univie.ac.at (B.K.K.). Fax: +43 1 4277 52630 (V.B.A.), +43 1 4277 52680 (B.K.K.).
† University of Vienna.
‡ Max-Planck-Institute of Biochemistry.

(1) Clarke, M. J. *Coord. Chem. Rev.* **2003**, *236*, 209−233.
(2) Debreczeni, J. E.; Bullock, A. N.; Atilla, G. E.; Williams, D. S.; Bregman, H.; Knapp, S.; Meggers, E. *Angew. Chem., Int. Ed.* **2006**, *45*, 1580−1585.
(3) Barve, V.; Ahmed, F.; Adsule, S.; Banerjee, S.; Kulkarni, S.; Katiyar, P.; Anson, C. E.; Powell, A. K.; Padhye, S.; Sarkar, F. *J. Med. Chem.* **2006**, *49*, 3800−3808.
(4) Schubert, J. *Sci. Am.* **1966**, *214*, 40−50.
(5) Rosenberg, B.; van Camp, L. *Cancer Res.* **1970**, *30*, 1799−1802.
(6) Anderegg, G.; Ripperger, H. *J. Chem. Soc., Chem. Commun.* **1989**, *47*, 647−650.
(7) Kamalakannan, P.; Venkappayya, D.; Balasubramanian, T. *J. Chem. Soc., Dalton Trans.* **2002**, *17*, 3381−3391.
(8) Cini, R.; Tamasi, G.; Defazio, S.; Corsini, M.; Zanello, P.; Messori, L.; Marcon, G.; Piccioli, M.; Orioli, P. *Inorg. Chem.* **2003**, *42*, 8038−8052.
(9) Fan, L.; Iyer, J.; Zhu, S.; Frick, K. K.; Wada, R. K.; Eskenazi, A. E.; Berg, P. E.; Ikegaki, N.; Kennett, R. H.; Frantz, C. N. *Cancer Res.* **2001**, *61*, 1073−1079.
(10) Pan, Q.; Kleer, C. G.; van Golen, K. L.; Irani, J.; Bottema, K. M.; Bias, C.; De Carvalho, M.; Mesri, E. A.; Robins, D. M.; Dick, R. D.; Brewer, G. J.; Merajver, S. D. *Cancer Res.* **2002**, *62*, 4854−4859.
(11) Abeysinghe, R. D.; Greene, B. T.; Haynes, R.; Willingham, M. C.; Turner, J.; Planalp, R. P.; Brechbiel, M. W.; Torti, F. M.; Torti, S. V. *Carcinogenesis* **2001**, *22*, 1607−1614.
(12) Lovejoy, D. B.; Richardson, D. R. *Curr. Med. Chem.* **2003**, *10*, 1035−1049.
(13) Arion, V. B.; Jakupec, M. A.; Galanski, M.; Unfried, P.; Keppler, B. K. *J. Inorg. Biochem.* **2002**, *91*, 298−305.
(14) Galanski, M.; Arion, V. B.; Jakupec, M. A.; Keppler, B. K. *Curr. Pharm. Des.* **2003**, *9*, 2078−2089.
(15) Timerbaev, A. R.; Hartinger, C. G.; Aleksenko, S. S.; Keppler, B. K. *Chem. Rev.* **2006**, *106*, 2224−2248.

10.1021/ic070098j CCC: $37.00
Published on Web 04/03/2007

Chart 1. Kenpaullone with the Atom Numbering Scheme

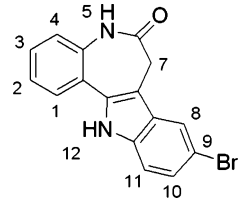

Of great interest in this regard is 9-bromo-7,12-dihydroindolo[3,2-*d*][1]benzazepin-6(5*H*)-one, kenpaullone (Chart 1),[16] which shows an activity profile similar to that of flavopiridol in vitro, a well-known inhibitor of cyclin-dependent kinases (CDKs).[17] A large number of kenpaullone derivatives have been documented by Kunick et al.[18,19] and some of them by us.[20] The structure−activity relationships have indicated certain features required for kinase-inhibiting potency, which does not necessarily parallel antiproliferative activity profile.[18,19,21] As a result, other intracellular targets for this class of compounds have also been suggested.[18,21−24]

One of the limitations encountered in the development of antitumor paullone derivatives is their low aqueous solubility and bioavailability. We expected that the imposed limitations could at least be diminished by complexation to metal ions, leading to improved pharmacokinetic and possibly, through synergistic effects with the metal ion, to enhanced pharmacodynamic properties. The effect of metalation of paullone compounds on both the antiproliferative activity and CDK-inhibitory activity is largely unexplored. Although the created library of paullone compounds is large, it contains only one metal-based derivative (vide infra).[20] This is primarily because paullone derivatives do not contain suitable metal-chelating sites. Their binding to metal ions could only be expected via lactam or thiolactam units with the formation of thermodynamically unfavored four-membered metallocycles.

By chemical modification of the thiolactam moiety in kenpaullone, a new derivative (HL) was obtained, which contains a tridentate N_2O binding site for gallium(III) (Scheme 1). The complex $[GaL_2]Cl{\cdot}2.5H_2O$ was found to be 1.5- to 18-fold more cytotoxic than HL. However, the low aqueous solubility and hydrolytic instability of this complex prompted us to search for other derivatives, in particular those able to chelate ruthenium species, since such complexes are expected to be kinetically more inert toward hydrolysis. The choice of the metal ion was also dictated by the fact that ruthenium complexes are known to possess antitumor properties. Of note are the ruthenium complexes $(H_2im)[trans\text{-}Ru^{III}Cl_4(Him)(DMSO)]$ (NAMI-A, DMSO = dimethyl sulfoxide; Him = imidazole) and $(H_2ind)[trans\text{-}Ru^{III}Cl_4(Hind)_2]$ (KP1019; Hind = indazole), which have finished phase I clinical trials, the former as an antimetastatic drug and the latter as an anticancer agent against primary tumors and metastases, in particular colon carcinomas.[25,26] Although the mechanism of action of both compounds has not yet been understood, DNA is considered as a possible target for KP1019.[25] Moreover, it has been proposed that in vivo reduction of Ru^{III} to the more reactive Ru^{II} is an important step in their mode of action.[27]

In vitro studies of paullones as well as KP1019 showed induction of apoptosis in tumor cells by the intrinsic mitochondrial pathway as indicated by perturbation of the mitochondrial membrane potential.[28−30] With this in mind, we focused our efforts on the synthesis of Ru^{II} complexes with bidentate paullone ligands with 1:1 and 1:2 metal-to-ligand ratios, which will presumably ensure strong metal−ligand bonding and preserve their ability to interact with DNA. For a chelating moiety to be attached to the paullone framework, α-picolylamine, an efficient chelating unit able to stabilize ruthenium(II) species, was chosen.

In this paper, we report on the syntheses, X-ray diffraction structures, and spectroscopic characterization of two novel paullone derivatives ($\mathbf{L^1}$ and $\mathbf{L^2}$). Both were obtained in high yield and purity (Scheme 1). We show that these ligands react with *cis*-$[Ru^{II}Cl_2(DMSO)_4]$ in 1:1 and 2:1 molar ratios, with the formation of stable molecular complexes *trans*-$[Ru^{II}Cl_2(DMSO)_2\mathbf{L^1}]$ (**1a**) and *trans*-$[Ru^{II}Cl_2(DMSO)_2\mathbf{L^2}]$ (**1b**) and ionic species $[Ru^{II}Cl(DMSO)(\mathbf{L^1})_2]Cl$ (**2a**) and $[Ru^{II}Cl(DMSO)(\mathbf{L^2})_2]Cl$ (**2b**), respectively. We found that upon complexation another tautomeric form of the ligands is stabilized. This is the first example of paullone ruthenation, which was confirmed by X-ray crystallographic studies of **1a**·2EtOH and **2b**·2.8EtOH·0.2H_2O. In addition, the cytotoxic activity of **2a** and **2b** in three human cancer cell lines in vitro and their influence on the DNA secondary structure are reported.

(16) Kunick, C. *Arch. Pharm. (Weinheim, Ger.*) **1992**, *325*, 297−299.
(17) Zaharewitz, D. W.; Gussio, R.; Leost, M.; Senderowitz, A. M.; Lahusen, T.; Kunick, C.; Meijer, L.; Sausville, E. A. *Cancer Res.* **1999**, *59*, 2566−2569.
(18) Schultz, C.; Link, A.; Leost, M.; Zaharevitz, D. W.; Gussio, R.; Sausville, E. A.; Meijer, L.; Kunick, C. *J. Med. Chem.* **1999**, *42*, 2909−2919.
(19) Kunick, C.; Schultz, C.; Lemcke, T.; Zaharevitz, D. W.; Gussio, R.; Jalluri, R. K.; Sausville, E. A.; Leost, M.; Meijer, L. *Bioorg. Med. Chem. Lett.* **2000**, *10*, 567−569.
(20) Dobrov, A.; Arion, V. B.; Kandler, N.; Ginzinger, W.; Jakupec, M. A.; Rufiñska, A.; Graf von Keyserlingk, N.; Galanski, M.; Kowol, C.; Keppler, B. K. *Inorg. Chem.* **2006**, *45*, 1945−1950.
(21) Pies, T.; Schaper, K.-J.; Leost, M.; Zaharevitz, D. W.; Gussio, R.; Meijer, L.; Kunick, C. *Arch. Pharm. (Weinheim, Ger.*) **2004**, *337*, 486−492.
(22) Wieking, K.; Knockaert, M.; Leost, M.; Zaharewitz, D. W.; Meijer, L.; Kunick, C. *Arch. Pharm. (Weinheim, Ger.*) **2002**, *7*, 311−317.
(23) Leost, M.; Schultz, C.; Link, A.; Wu, Y. Z.; Biernat, J.; Mandelkow, E. M.; Bibb, J. A.; Snyder, G. L.; Greengard, P.; Zaharewitz, D. W.; Gussio, R.; Senderowicz, A. M.; Sausville, E. A.; Kunick, C.; Meijer, L. *Eur. J. Biochem.* **2000**, *267*, 5983−5994.
(24) Knockaert, M.; Wieking, K.; Schmitt, S.; Leost, M.; Grant, K. M.; Mottram, J. C.; Kunick, C.; Meijer, L. *J. Biol. Chem.* **2002**, *277*, 25493−25501.
(25) Hartinger, C. G.; Zorbas-Seifried, S.; Jakupec, M. A.; Kynast, B.; Zorbas, H.; Keppler, B. K. *J. Inorg. Biochem.* **2006**, *100*, 891−904.
(26) Alessio, E.; Mestroni, G.; Bergamo, B.; Sava, G. *Curr. Top. Med. Chem.* **2004**, *4*, 1525−1535.
(27) Reisner, E.; Arion, V. B.; Guedes da Silva, M. F. C.; Lichtenecker, R.; Eichinger, A.; Keppler, B. K.; Kukushkin, V. Y.; Pombeiro, A. J. L. *Inorg. Chem.* **2004**, *43*, 7083−7093.
(28) Lahusen, T.; De Siervi, A.; Kunick, C.; Senderowicz, A. M. *Mol. Carcinog.* **2003**, *36*, 183−194.
(29) Kapitza, S.; Jakupec, M.; Weiss, M.; Keppler, B. K.; Marian, B. *J. Cancer Res. Clin. Oncol.* **2001**, *127*, S45.
(30) Kapitza, S.; Jakupec, M.; Weiss, M.; Keppler, B. K.; Marian, B. *Proc. Am. Assoc. Cancer Res.* **2001**, *42*, 214.

Scheme 1. Syntheses of Lactam-Modified Paullone Ligands and Their Complexes[a]

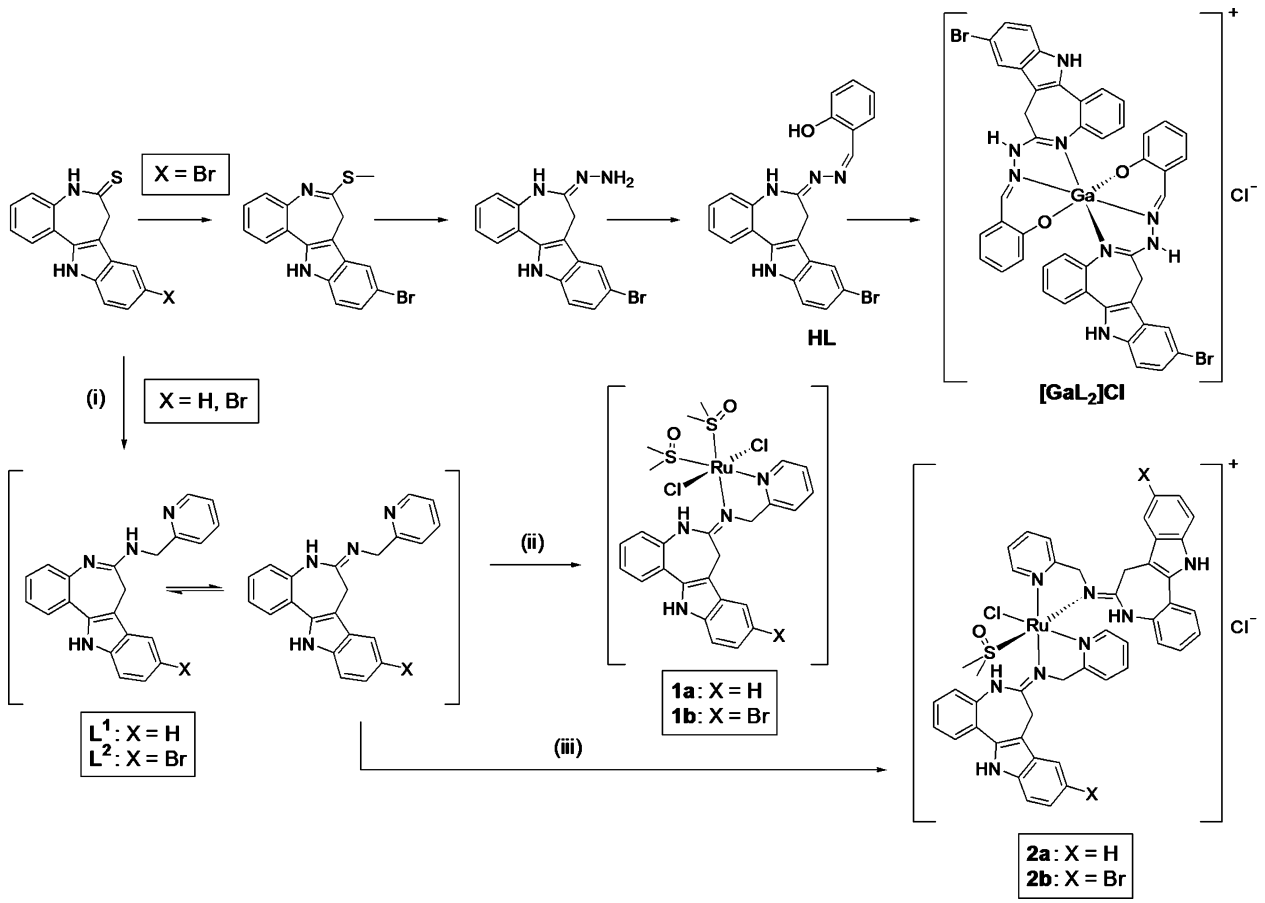

[a] Reagents and conditions: upper synthesis route (see ref 20) (i) 2 equiv of α-picolylamine, THF_{abs}, reflux, 24 h, 90% (**L**[1]), 95% (**L**[2]); (ii) *cis*-[$RuCl_2(DMSO)_4$], $EtOH_{abs}$, 50 °C, 6 h, 26% (**1a**), 30% (**1b**); (iii) 0.5 equiv of *cis*-[$RuCl_2(DMSO)_4$], EtOH, 75 °C, 6 h, 16% (**2a**), 23% (**2b**).

Experimental Section

Starting Materials. 7,12-Dihydroindolo[3,2-*d*][1]benzazepin-6(5*H*)-thione, 9-bromo-7,12-dihydroindolo[3,2-*d*][1]benzazepin-6(5*H*)-thione,[18] and *cis*-[$RuCl_2(DMSO)_4$][31] have been prepared following the published protocols. Tetrahydrofuran (THF) and ethanol were dried using standard procedures. α-Picolylamine was purchased from Acros and used without further purification.

Synthesis of Novel Ligands and Ruthenium(II) Complexes. 6-(α-Picolylamino)-7,12-dihydroindolo[3,2-*d*][1]benzazepine (L[1]). To 7,12-dihydroindolo[3,2-*d*][1]benzazepin-6(5*H*)-thione (3.00 g, 11.3 mmol) in dry THF (120 mL) was added α-picolylamine (2.4 mL, 23.2 mmol), and the solution was refluxed for 24 h. After cooling to room temperature, the mixture was filtered and the solvent was removed under reduced pressure. The resulting solid was washed with acetone (6 × 20 mL) and dried in vacuo at 80 °C, yielding **L**[1] as a white solid. Further fractions were obtained by concentrating the acetone solution to about half the original volume and inducing crystallization at −20 °C. The resulting crystals were washed with diethyl ether (2 × 10 mL) and dried in vacuo at 80 °C. Yield: 3.44 g, 90%. Anal. Calcd for $C_{22}H_{18}N_4$: C, 78.08; H, 5.36; N, 16.56. Found: C, 77.89; H, 5.13; N, 16.52. ESI-MS, *m*/*z*, positive: 339 [**L**[1] + H]$^+$; negative, 337 [**L**[1] − H]$^-$. IR spectrum, selected bands, KBr, ν_{max}, cm^{-1}: 3414 (NH), 3227 (NH), 3055 (CH_{arom}), 1615 (CN), 1596, 1558, 1548, 743 (CH_{arom}). UV−vis spectrum, methanol, λ_{max}, nm (ϵ, $dm^3\ mol^{-1}\ cm^{-1}$): 237 (36520), 262 (29870), 268 (30090), 314 (20070). ^{1}H NMR (400.13 MHz), DMSO-d_6, δ_H, ppm: 3.44 (s, 2H, H^7), 4.52 (d, ^3J = 5.3 Hz, 2H, H^{14}), 7.04 (t, ^3J = 7.4 Hz, 1H, H^2), 7.08 (m, 1H, H^9), 7.09 (d, ^3J = 8.2 Hz, 1H, H^4), 7.15 (t, ^3J = 7.5 Hz, 1H, H^{10}), 7.22 (m, 2H, H^3, H^{17}), 7.30 (d, ^3J = 7.9 Hz, 1H, H^{15}), 7.43 (d, ^3J = 8.0 Hz, 1H, H^{11}), 7.66 (t, ^3J = 7.6 Hz, 1H, H^{16}), 7.67 (d, ^3J = 7.6 Hz, 1H, H^8), 7.71 (d, ^3J = 7.8 Hz, 1H, H^1), 7.86 (t, ^3J = 5.3 Hz, 1H, H^{13}), 8.50 (d, ^3J = 4.7 Hz, 1H, H^{18}), 11.42 (s, 1H, H^{12}). ^{13}C NMR (100.63 MHz), DMSO-d_6, δ_C, ppm: 28.84 (C^7), 47.44 (C^{14}), 109.75 (C^{7a}), 112.08 (C^{11}), 118.62 (C^8), 119.54 (C^9), 121.32 (C^2), 122.33 (C^{10}, C^{15}), 122.85 (C^{17}), 123.27 (C^{12b}), 127.33 (C^{7b}), 127.35 (C^1), 127.78 (C^3), 128.28 (C^4), 134.61 (C^{12a}), 137.36 (C^{16}), 138.23 (C^{11a}), 146.64 (C^{4a}), 149.63 (C^{18}), 155.50 (C^6), 159.64 (C^{14a}). ^{15}N NMR (40.55 MHz), DMSO-d_6, δ_N, ppm: 77.3 (N^{13}), 105.0 (N^{12}). Single crystals suitable for X-ray diffraction study were obtained by slow diffusion of pentane into a solution of **L**[1] in THF.

9-Bromo-6-(α-picolylamino)-7,12-dihydroindolo[3,2-*d*][1]-benzazepine (L[2]). To 9-bromo-7,12-dihydroindolo[3,2-*d*][1]-benzazepin-6(5*H*)-thione (3.00 g, 8.7 mmol) in dry THF (150 mL) was added α-picolylamine (1.8 mL, 15.6 mmol), and the solution was refluxed for 24 h. After cooling to room temperature, the mixture was filtered, concentrated to about half the original volume, and left to stand at −20 °C. The resulting white crystals were washed with diethyl ether (3 × 10 mL) and dried in vacuo at 80 °C. Further fractions were obtained upon concentration of the THF solution and crystallization at −20 °C. Yield: 3.45 g, 95%. Anal. Calcd for $C_{22}H_{17}BrN_4$: C, 63.32; H, 4.11; Br, 19.15; N, 13.43. Found: C, 63.04; H, 4.25; Br, 19.17; N, 13.21. ESI-MS, *m*/*z*,

(31) Evans, I. P.; Spencer, A.; Wilkinson, G. *Dalton Trans.* **1973**, 204−209.

positive: 419 [**L²** + H]⁺; negative, 417 [**L²** − H]⁻. IR spectrum, selected bands, KBr, ν_{max}, cm^{-1}: 3421 (NH), 3214 (NH), 3053 (CH_{arom}), 1612 (CN), 1597, 1558, 760 (CH_{arom}). UV−vis spectrum, methanol, λ_{max}, nm (ϵ, dm^3 mol^{-1} cm^{-1}): 239 (36370), 260 (29260), 319 (17460). ^{1}H NMR (400.13 MHz), DMSO-d_6, δ_H, ppm: 3.41 (s, 2H, H^7), 4.51 (d, ^3J = 5.3 Hz, 2H, H^{14}), 7.05 (t, ^3J = 7.4 Hz, 1H, H^2), 7.09 (d, ^3J = 8.0 Hz, 1H, H^4), 7.24 (m, 3H, H^3, H^{10}, H^{17}), 7.30 (d, ^3J = 7.8 Hz, 1H, H^{15}), 7.38 (d, ^3J = 8.6 Hz, 1H, H^{11}), 7.68 (t, ^3J = 7.7 Hz, 1H, H^{16}), 7.69 (d, ^3J = 7.8 Hz, 1H, H^1), 7.81 (t, ^3J = 5.3 Hz, 1H, H^{13}), 7.86 (s, 1H, H^8), 8.51 (d, ^3J = 4.7 Hz, 1H, H^{18}), 11.65 (s, 1H, H^{12}). ^{13}C NMR (100.63 MHz), DMSO-d_6, δ_C, ppm: 28.60 (C^7), 47.44 (C^{14}), 109.26 (C^{7a}), 112.08 (C^9), 114.03 (C^{11}), 120.97 (C^8), 121.38 (C^2), 122.40 (C^{15}), 122.70 (C^{12b}), 122.92 (C^{17}), 124.59 (C^{10}), 127.46 (C^1), 128.28 (C^3), 128.34 (C^4), 129.06 (C^{7b}), 136.22 (C^{12a}), 136.83 (C^{11a}), 137.41 (C^{16}), 146.92 (C^{4a}), 149.67 (C^{18}), 155.40 (C^6), 159.41 (C^{14a}). ^{15}N NMR (40.55 MHz), DMSO-d_6, δ_N, ppm: 77.4 (N^{13}), 107.2 (N^{12}). X-ray-diffraction-quality single crystals were grown by slow diffusion of hexane into a THF solution of **L²**.

(*OC*-6-14)-Dichlorobis(dimethyl sulfoxide)(6-(*E*)-[(α-picolyl-κ*N*)imino-κ*N*]-7,12-dihydroindolo[3,2-*d*][1]benzazepine)-ruthenium(II), *trans*-[Ru^{II}Cl$_2$(DMSO)$_2$L^1] (1a). A mixture of *cis*-[$RuCl_2(DMSO)_4$] (0.49 g, 1.0 mmol) and **L¹** (0.34 g, 1.0 mmol) in dry ethanol (20 mL) was stirred at 50 °C for 6 h and then allowed to cool down to room temperature. The yellow precipitate was filtered off, washed with dry ethanol (2 × 5 mL), and dried in vacuo. Yield: 0.17 g, 26%. Anal. Calcd for $C_{26}H_{30}Cl_2N_4O_2RuS_2$: C, 46.84; H, 4.54; Cl, 10.64; N, 8.40; S, 9.62. Found: C, 46.82; H, 4.60; Cl, 10.64; N, 8.31; S, 9.46. ESI-MS, *m*/*z*, positive: 691 [**1a** + Na]⁺, 631 [**1a** − Cl]⁺, 611 [**1a** − DMSO + Na]⁺; negative, 703 [**1a** + Cl]⁻, 625 [**1a** − DMSO + Cl]⁻. IR spectrum (cm^{-1}), selected bands, ν_{max}: KBr, 3467 (NH), 3253 (NH), 3169, 3075 (CH_{arom}), 1627 (CN), 1090, 1083 (SO), 1057, 765, 746 (CH_{arom}); CsI, 449, 429 (RuS), 395 (CSO). UV−vis spectrum, methanol, λ_{max}, nm (ϵ, dm^3 mol^{-1} cm^{-1}): 229 (36330), 259 (28260), 303 (26020). ^{1}H NMR (400.13 MHz), DMSO-d_6, δ_H, ppm: 2.62 (broad s, 6H, CH_3), 3.23 (broad s, 6H, CH_3), 4.99 (broad s, 2H, H^7), 5.72 (s, 2H, H^{14}), 7.07 (d, ^3J = 8.0 Hz, 1H, H^4), 7.16 (t, ^3J = 7.4 Hz, 1H, H^9), 7.23 (t, ^3J = 7.4 Hz, 1H, H^{10}), 7.28 (t, ^3J = 7.5 Hz, 1H, H^2), 7.42 (t, ^3J = 7.5 Hz, 1H, H^3), 7.48 (m, 1H, H^{17}), 7.49 (m, 1H, H^{11}), 7.66 (d, ^3J = 7.6 Hz, 1H, H^{15}), 7.84 (d, ^3J = 7.9 Hz, 1H, H^1), 7.90 (d, ^3J = 7.8 Hz, 1H, H^8), 7.96 (t, ^3J = 7.4 Hz, 1H, H^{16}), 10.01 (d, ^3J = 5.6 Hz, 1H, H^{18}), 10.50 (s, 1H, H^5), 11.75 (s, 1H, H^{12}). ^{13}C NMR (100.63 MHz), DMSO-d_6, δ_C, ppm: 25.11 (C^7), 59.89 (C^{14}), 108.10 (C^{7a}), 112.55 (C^{11}), 119.00 (C^8), 120.45 (C^9), 120.68 (C^4), 121.52 (C^{15}), 121.86 (C^{12b}), 122.95 (C^{17}), 123.47 (C^{10}), 124.21 (C^2), 127.09 (C^{7b}), 128.35 (C^1), 129.58 (C^3), 133.95 (C^{12a}), 135.82 (C^{4a}), 138.42 (C^{11a}), 138.46 (C^{16}), 155.33 (C^{18}), 165.43 (C^{14a}), 165.89 (C^6), no CH_3 resonances detected. ^{15}N NMR (40.55 MHz), DMSO-d_6, δ_N, ppm: 105.9 (N^5), 107.7 (N^{12}). Single crystals of **1a**·2EtOH suitable for X-ray diffraction study could be selected directly from the reaction vessel.

(*OC*-6-14)-(9-Bromo-6-(*E*)-[(α-picolyl-κ*N*)imino-κ*N*]-7,12-dihydroindolo[3,2-*d*][1]benzazepine)dichlorobis(dimethyl sulfoxide)ruthenium(II), *trans*-[Ru^{II}Cl$_2$(DMSO)$_2$L^2] (1b). A mixture of *cis*-[$RuCl_2(DMSO)_4$] (0.49 g, 1.0 mmol) and **L²** (0.42 g, 1.0 mmol) in dry ethanol (25 mL) was stirred at 50 °C for 6 h and then allowed to cool to room temperature. The yellow precipitate was filtered off, washed with dry ethanol (2 × 5 mL), and dried in vacuo. Yield: 0.22 g, 30%. Anal. Calcd for $C_{26}H_{29}BrCl_2N_4O_2RuS_2$: C, 41.89; H, 3.92; Br, 10.72; Cl, 9.51; N, 7.51; S, 8.60. Found: C, 41.40; H, 3.85; Br, 10.64; Cl, 9.30; N, 7.33; S, 8.40. ESI-MS, *m*/*z*, positive: 785 [**1b** + K]⁺, 769 [**1b** + Na]⁺; negative, 781 [**1b** + Cl]⁻, 745 [**1b** − H]⁻, 667 [**1b** − DMSO − H]⁻, 589 [**1b** − 2DMSO − H]⁻. IR spectrum (cm^{-1}), selected bands, ν_{max}: KBr, 3437 (NH), 3246, 3227 (NH), 1626 (CN), 1581, 1569, 1400, 1091, 1071 (SO), 1056, 764 (CH_{arom}); CsI, 447, 426 (RuS), 398 (CSO). UV−vis spectrum, methanol, λ_{max}, nm (ϵ, dm^3 mol^{-1} cm^{-1}): 235 (30320), 258 (23140), 312 (18690). ^{1}H NMR (400.13 MHz), DMSO-d_6, δ_H, ppm: 2.66 (broad s, 6H, CH_3), 3.23 (broad s, 6H, CH_3), 4.97 (broad s, 2H, H^7), 5.72 (s, 2H, H^{14}), 7.07 (d, ^3J = 8.0 Hz, 1H, H^4), 7.28 (t, ^3J = 7.5 Hz, 1H, H^2), 7.33 (d, ^3J = 8.6 Hz, 1H, H^{10}), 7.44 (m, 1H, H^3), 7.45 (d, ^3J = 8.6 Hz, 1H, H^{11}), 7.48 (m, 1H, H^{17}), 7.63 (d, ^3J = 7.6 Hz, 1H, H^{15}), 7.83 (d, ^3J = 7.5 Hz, 1H, H^1), 7.97 (t, ^3J = 7.6 Hz, 1H, H^{16}), 8.17 (s, 1H, H^8), 10.00 (d, ^3J = 5.4 Hz, 1H, H^{18}), 10.52 (s, 1H, H^5), 11.98 (s, 1H, H^{12}). ^{13}C NMR (100.63 MHz), DMSO-d_6, δ_C, ppm: 24.94 (C^7), 60.06 (C^{14}), 107.58 (C^{7a}), 113.05 (C^9), 114.56 (C^{11}), 120.71 (C^4), 121.30 (C^{12b}), 121.33 (C^8), 121.46 (C^{15}), 122.99 (C^{17}), 124.26 (C^2), 125.93 (C^{10}), 128.47 (C^1), 128.88 (C^{7b}), 130.03 (C^3), 135.48 (C^{12a}), 136.05 (C^{4a}), 137.02 (C^{11a}), 138.51 (C^{16}), 155.35 (C^{18}), 165.38 (C^{14a}), 165.95 (C^6), no CH_3 resonances detected. ^{15}N NMR (40.55 MHz), DMSO-d_6, δ_N, ppm: 105.9 (N^5), 109.5 (N^{12}).

(*OC*-6-43)-Chloro(dimethyl sulfoxide)bis(6-(*E*)-[(α-picolyl-κ*N*)imino-κ*N*]-7,12-dihydroindolo[3,2-*d*][1]benzazepine)ruthenium-(II) Chloride Sesquihydrate, [Ru^{II}Cl(DMSO)(L^1)$_2$]Cl·1.5H$_2$O (2a·1.5H$_2$O). A mixture of *cis*-[$RuCl_2(DMSO)_4$] (0.49 g, 1.0 mmol) and **L¹** (0.68 g, 2.0 mmol) in ethanol (54 mL) was stirred at 75 °C for 6 h, whereupon the solution was concentrated under reduced pressure to a final volume of 20 mL and left to stand at −20 °C for 2 weeks. The yellow crystals were filtered off and washed with ethanol (1 × 3 mL). On drying in vacuo, a microcrystalline powder is formed. Yield: 0.15 g, 16%. Anal. Calcd for $C_{46}H_{42}Cl_2N_8ORuS\cdot 1.5H_2O$: C, 57.92; H, 4.75; Cl, 7.43; N, 11.75; S, 3.36. Found: C, 57.37; H, 4.58; Cl, 7.41; N, 11.48; S, 3.31. ESI-MS, *m*/*z*, positive: 891 [cation **2a**]⁺, 813 [cation **2a** − DMSO]⁺. IR spectrum (cm^{-1}), selected bands, ν_{max}: KBr, 3402 (NH), 3147 (NH), 1626 (CN), 1575, 1565, 1489, 1399, 1080 (SO), 1058, 1009, 741 (CH_{arom}); CsI, 466, 429 (RuS), 397 (CSO). UV−vis spectrum, methanol, λ_{max}, nm (ϵ, dm^3 mol^{-1} cm^{-1}): 230 (43690), 300 (24620). ^{1}H NMR (400.13 MHz), DMSO-d_6, δ_H, ppm: 1.56 (s, 3H, CH_3), 1.87 (d, ^2J = 14.9 Hz, 1H, H^{14} or H$^{14'}$), 3.05 (s, 3H, CH_3), 3.29 (m, 2H, H^7 or H$^{7'}$, H^{14} or H$^{14'}$), 3.75 (d, ^2J = 17.1 Hz, 1H, H^7 or H$^{7'}$), 4.11 (d, ^2J = 14.9 Hz, 1H, H^{14} or H$^{14'}$), 4.85 (d, ^2J = 14.6 Hz, 1H, H^{14} or H$^{14'}$), 4.95 (d, ^2J = 18.8 Hz, 1H, H^7 or H$^{7'}$), 5.68 (d, ^2J = 17.4 Hz, 1H, H^7 or H$^{7'}$), 6.53 (d, ^3J = 7.8 Hz, 1H, H_{arom}), 7.03 (d, ^3J = 7.4 Hz, 1H, H_{arom}), 7.04 (m, 2H, H_{arom}), 7.09 (m, 3H, H_{arom}), 7.18 (m, 2H, H_{arom}), 7.31 (t, ^3J = 7.5 Hz, 1H, H_{arom}), 7.51 (t, ^3J = 7.1 Hz, 1H, H_{arom}), 7.53 (d, ^3J = 8.3 Hz, 1H, H_{arom}), 7.57 (d, ^3J = 6.7 Hz, 1H, H_{arom}), 7.59 (m, 2H, H_{arom}), 7.63 (d, ^3J = 7.9 Hz, 1H, H_{arom}), 7.67 (d, ^3J = 8.2 Hz, 1H, H_{arom}), 7.73 (d, ^3J = 7.9 Hz, 1H, H_{arom}), 7.76 (d, ^3J = 7.8 Hz, 1H, H_{arom}), 9.01 (d, ^3J = 5.4 Hz, 1H, H^{18} or H$^{18'}$), 9.51 (s, 1H, H^5 or H$^{5'}$), 10.68 (s, 1H, H^5 or H$^{5'}$), 11.72 (s, 1H, H^{12} or H$^{12'}$), 11.99 (s, 1H, H^{12} or H$^{12'}$). ^{13}C NMR (100.63 MHz), DMSO-d_6, δ_C, ppm: 22.90 (C^7 or C$^{7'}$), 25.17 (C^7 or C$^{7'}$), 41.85 (CH_3), 45.75 (CH_3), 58.02 (C^{14} or C$^{14'}$), 59.93 (C^{14} or C$^{14'}$), 106.49 (C^{7a} or C$^{7a'}$), 112.60 (C^{11} or C$^{11'}$), 112.93 (C^{11} or C$^{11'}$), 119.07, 119.12, 120.34, 120.53, 120.73, 121.55, 121.58 (C^{12b} or C$^{12b'}$), 121.84, 122.04, 122.98 (C^{12b} or C$^{12b'}$), 123.27, 124.36 (2C), 124.70, 125.22, 126.21 (C^{7b} or C$^{7b'}$), 126.79 (C^{7b} or C$^{7b'}$), 128.33 (2C, C^1 and C$^{1'}$), 129.27 (C^3 or C$^{3'}$), 129.71 (C^3 or C$^{3'}$), 134.00 (C^{12a} or C$^{12a'}$), 134.28 (C^{12a} or C$^{12a'}$), 135.70 (C^{4a} or C$^{4a'}$), 135.82 (C^{4a} or C$^{4a'}$), 137.63 (C^{16} or C$^{16'}$), 138.18 (C^{11a} or C$^{11a'}$), 138.22 (C^{16} or C$^{16'}$), 139.05 (C^{11a} or C$^{11a'}$), 152.69 (C^{18} or C$^{18'}$), 157.32 (C^{18} or C$^{18'}$), 163.18 (C$^{6'}$ or C^{14a} or C$^{14a'}$), 163.62 (C$^{6'}$ or C^{14a} or C$^{14a'}$), 163.88 (C$^{6'}$ or C^{14a} or C$^{14a'}$), 167.35 (C^6).

(*OC*-6-43)-Bis(9-bromo-6-(*E*)-[(α-picolyl-κ*N*)imino-κ*N*]-7,12-dihydroindolo[3,2-*d*][1]benzazepine)chloro(dimethyl sulfoxide)-ruthenium(II) Chloride Sesquihydrate, [Ru^{II}Cl(DMSO)($\mathbf{L^2}$)$_2$]Cl·1.5H$_2$O (2b·1.5H$_2$O). A mixture of *cis*-[RuCl$_2$(DMSO)$_4$] (0.49 g, 1.0 mmol) and $\mathbf{L^2}$ (0.84 g, 2.0 mmol) in ethanol (54 mL) was stirred at 75 °C for 6 h, and the resulting solution was left to stand at −20 °C for 2 weeks. The yellow crystals were filtered off and washed with ethanol (1 × 3 mL). On drying in vacuo, a microcrystalline powder is formed. Yield: 0.26 g, 23%. Anal. Calcd for $C_{46}H_{40}Br_2Cl_2N_8ORuS\cdot1.5H_2O$: C, 49.70; H, 3.90; Br, 14.37; Cl, 6.38; N, 10.08; S, 2.88. Found: C, 49.70; H, 3.88; Br, 14.28; Cl, 6.35; N, 10.11; S, 2.93. ESI-MS, *m*/*z*, positive: 1049 [cation **2b**]$^+$, 971 [cation **2b** − DMSO]$^+$; negative, 1047 [cation **2b** − 2H]$^-$, 969 [cation **2b** − DMSO − 2H]$^-$, 933 [cation **2b** − DMSO − Cl − 3H]$^-$. IR spectrum (cm^{-1}), selected bands, ν_{max}: KBr, 3414 (NH), 3159 (NH), 1627 (CN), 1566, 1481, 1465, 1399, 1073 (SO), 1059, 764 (CH$_{arom}$); CsI, 466, 430 (RuS), 400 (CSO). UV−vis spectrum, methanol, λ_{max}, nm (ϵ, dm^3 mol^{-1} cm^{-1}): 234 (64310), 314 (31970). ^{1}H NMR (400.13 MHz), DMSO-d_6, δ_H, ppm: 1.69 (s, 3H, CH$_3$), 3.08 (s, 3H, CH$_3$); paullone ligand 1 (N^{13} trans to DMSO), 2.01 (d, ^3J = 15.0 Hz, 1H, H^{14}), 3.45 (d, ^3J = 18.8 Hz, 1H, H^7), 4.18 (d, ^3J = 14.8 Hz, 1H, H^{14}), 5.17 (d, ^3J = 18.9 Hz, 1H, H^7), 6.71 (d, ^3J = 7.8 Hz, 1H, H^{15}), 7.11 (t, ^3J = 7.0 Hz, 1H, H^{17}), 7.21 (d, ^3J = 8.6 Hz, 1H, H^{10}), 7.27 (d, ^3J = 5.6 Hz, 1H, H^{18}), 7.36 (d, ^3J = 8.5 Hz, 1H, H^{11}), 7.37 (t, ^3J = 7.5 Hz, 1H, H^2), 7.58 (t, ^3J = 7.7 Hz, 1H, H^3), 7.59 (m, 2H, H^4, H$^{15'}$), 7.67 (t, ^3J = 7.7 Hz, 1H, H^{16}), 7.80 (d, ^3J = 7.5 Hz, 1H, H^1), 8.03 (s, 1H, H^8), 10.74 (s, 1H, H^5), 12.15 (s, 1H, H^{12}); paullone ligand 2 (N$^{19'}$ trans to Cl), 3.31 (d, ^3J = 14.4 Hz, 1H, H$^{14'}$), 3.80 (d, ^3J = 17.7 Hz, 1H, H$^{7'}$), 4.87 (d, ^3J = 14.2 Hz, 1H, H$^{14'}$), 5.70 (d, ^3J = 17.6 Hz, 1H, H$^{7'}$), 7.03 (d, ^3J = 7.9 Hz, 1H, H$^{4'}$), 7.07 (t, ^3J = 7.8 Hz, 1H, H$^{3'}$), 7.17 (t, ^3J = 7.4 Hz, 1H, H$^{2'}$), 7.40 (d, ^3J = 8.7 Hz, 1H, H$^{10'}$), 7.53 (t, ^3J = 6.7 Hz, 1H, H$^{17'}$), 7.59 (m, 2H, H$^{15'}$, H^4), 7.62 (d, ^3J = 8.6 Hz, 1H, H$^{11'}$), 7.88 (d, ^3J = 7.6 Hz, 1H, H$^{1'}$), 7.92 (s, 1H, H$^{8'}$), 7.99 (t, ^3J = 7.7 Hz, 1H, H$^{16'}$), 9.04 (d, ^3J = 5.4 Hz, 1H, H$^{18'}$), 9.42 (s, 1H, H$^{5'}$), 12.32 (s, 1H, H$^{12'}$). ^{13}C NMR (100.63 MHz), DMSO-d_6, δ_C, ppm: 42.10 (CH$_3$), 45.78 (CH$_3$); paullone ligand 1 (N^{13} trans to DMSO), 22.90 (C^7), 59.33 (C^{14}), 105.98 (C^{7a}), 112.96 (C^9), 114.53 (C^{11}), 120.85 (C^{15}), 121.12 (C^{12b}), 121.50 (C^8), 121.86 or 122.04 (C^4), 124.42 (C^{17}), 125.29 (C^2), 125.77 (C^{10}), 128.12 (C^{7b}), 128.52 or 128.68 (C^1), 130.12 (C^3), 135.54 (C^{12a}), 136.05 (C^{4a}), 136.82 (C^{11a}), 137.68 (C^{16}), 152.92 (C^{18}), 163.85 (C^{14a}), 167.75 (C^6); paullone ligand 2 (N$^{19'}$ trans to Cl), 24.93 (C$^{7'}$), 58.28 (C$^{14'}$), 108.15 (C$^{7a'}$), 113.16 (C$^{9'}$), 114.91 (C$^{11'}$), 121.43 (C$^{8'}$), 121.50 (C$^{4'}$), 121.86 or 122.04 (C$^{15'}$), 122.55 (C$^{12b'}$), 124.42 (C$^{2'}$), 124.74 (C$^{17'}$), 126.09 (C$^{10'}$), 128.52 or 128.68 (C$^{1'}$), 128.68 (C$^{7b'}$), 129.59 (C$^{3'}$), 135.76 (C$^{12a'}$), 136.88 (C$^{4a'}$), 137.55 (C$^{11a'}$), 138.26 (C$^{16'}$), 157.34 (C$^{18'}$), 163.75 (C$^{6'}$), 163.85 (C$^{14a'}$). ^{15}N NMR (40.55 MHz), DMSO-d_6, δ_N, ppm: paullone ligand 1, 108.2 (N^5), 110.6 (N^{12}); paullone ligand 2, 103.5 (N$^{5'}$), 110.8 (N$^{12'}$). Single crystals of **2b**·2.8EtOH·0.2H$_2$O suitable for X-ray diffraction study could be selected directly from the reaction vessel.

Physical Measurements. ^{1}H, ^{31}P, ^{13}C, NOE difference and two-dimensional ^{1}H−^{1}H COSY, ^{1}H−^{1}H TOCSY, ^{1}H−^{13}C HMQC, ^{1}H−^{13}C HMBC, and ^{1}H−^{15}N HMQC NMR spectra were recorded with a Bruker Avance DPX 400 spectrometer (Ultrashield Magnet) in DMSO-d_6 at 25 °C using standard pulse programs at 400.13 (^{1}H), 161.98 (^{31}P), 100.63 (^{13}C), and 40.55 MHz (^{15}N). Two-dimensional spectra were measured in a gradient-enhanced mode. ^{1}H and ^{13}C shifts are referenced relative to the solvent signals, and ^{15}N shifts are given relative to those of external NH$_4$Cl. Elemental analyses were carried out by the Microanalytical Service at the Institute of Physical Chemistry of the University of Vienna. Infrared spectra were recorded on a Perkin-Elmer FT-IR 2000 spectrometer in KBr (4000−400 cm^{-1}) and CsI pellets (600−200 cm^{-1}). UV−vis spectra were measured on a Perkin-Elmer Lambda 650 UV−vis spectrophotometer using samples dissolved in methanol, methanol−water or DMSO−water. Electrospray ionization mass spectrometry (ESI-MS) was carried out with a Bruker Esquire 3000 instrument (Bruker Daltonic, Bremen, Germany). Expected and experimental isotope distributions were compared. Values of *m*/*z* are quoted for the species with the highest natural abundance. Conductivity measurements were performed with a LF 538 WTW conductivity meter. Cyclic voltammograms were measured in a two-compartment three-electrode cell using a 0.5 mm diameter platinum-disk working electrode or alternatively with a glassy-carbon electrode (diameter = 1.0 mm), probed by a Luggin capillary connected to a silver wire pseudo-reference-electrode and a platinum auxiliary electrode. Measurements were performed at room temperature using an EG&G PARC 273A potentiostat/galvanostat. Deaeration of the solutions was accomplished by passing a stream of high-purity nitrogen through the solution for 10 min prior to the measurements and then maintaining a blanket atmosphere of nitrogen over the solution during the measurements. The potentials were measured in 0.2 M [*n*-Bu$_4$N][BF$_4$]/DMF at a scan rate of 200 mV/s, employing a platinum-disk working electrode.

Crystallographic Structure Determination. X-ray diffraction measurements were performed on Nonius Kappa CCD ($\mathbf{L^1}$) and Bruker X8 APEXII CCD diffractometers ($\mathbf{L^2}$, **1a**·2EtOH, and **2b**·2.8EtOH·0.2H$_2$O) at 120 and 100 K, respectively. Single crystals were positioned at 30, 37.5, 50, and 37.5 mm from the detector, and 484, 1318, 1121, and 919 frames were measured, each for 25, 50, 60, and 20 s over 1.5°, 1°, 1°, and 1° scan widths for $\mathbf{L^1}$, $\mathbf{L^2}$, **1a**·2EtOH, and **2b**·2.8EtOH·0.2H$_2$O, correspondingly. The data were processed using *Denzo-SMN*[32] and *SAINT* software.[33] Crystal data, data collection parameters, and structure refinement details are given in Table 1. The structures were solved by direct methods and refined by full-matrix least-squares techniques. Non-H atoms were refined with anisotropic displacement parameters. H atoms were inserted in calculated positions and refined with a riding model. The following computer programs and equipment were used: structure solution, *SHELXS-97*;[34] refinement, *SHELXL-97*;[35] molecular diagrams, *SCHAKAL-97*;[36] computer, Pentium IV; scattering factors.[37]

Computational Details. Gas-phase optimization of the molecular structure of $\mathbf{L^1}$ was performed using the geometry of the ligand resulting from an X-ray diffraction study as the starting point. The calculations were carried out at the density functional level of theory with Becke's three-parameter hybrid functional[38] using the correlation functional of Lee, Yang, and Parr[39,40] (B3LYP), as

(32) Otwinowski, Z.; Minor, W. Processing of X-ray Diffraction Data Collected in Oscillation Mode. In *Methods in Enzymology, Macromolecular Crystallography*; Carter, C. W., Jr., Sweet, R. M., Eds.; Academic Press: New York, 1997; Vol. 276, Part A, pp 307−326.

(33) Pressprich, M. R.; Chambers, J. *SAINT+ Integration Engine, Program for Crystal Structure Integration*; Bruker Analytical X-ray Systems: Madison, WI, 2004.

(34) Sheldrick, G. M., *SHELXS-97, Program for Crystal Structure Solution*; University of Göttingen: Göttingen, Germany, 1997.

(35) Sheldrick, G. M., *SHELXL-97, Program for Crystal Structure Refinement*; University of Göttingen: Göttingen, Germany, 1997.

(36) Keller, E. *SCHAKAL-97*; Kristallographisches Institut, Universität Freiburg: Freiburg, Germany, 1997.

(37) *International Tables for X-ray Crystallography*; Kluwer Academic Press: Dordrecht, The Netherlands, 1992; Vol. C, Tables 4.2.6.8 and 6.1.1.4.

(38) Becke, A. D. *J. Chem. Phys.* **1993**, *98*, 5648−5652.

(39) Lee, C.; Yang, W.; Parr, R. G. *Phys. Rev. B* **1988**, *37*, 785−789.

(40) Miehlich, B.; Savin, A.; Stoll, H.; Preuss, H. *Chem. Phys. Lett.* **1989**, *157*, 200−206.

Table 1. Crystal Data and Details of Data Collection for $\mathbf{L^1}$, $\mathbf{L^2}$, **1a**·2EtOH, and **2b**·2.8EtOH·0.2H_2O

	compound			
	$\mathbf{L^1}$	$\mathbf{L^2}$	**1a**·2EtOH	**2b**·2.8EtOH·0.2H_2O
chemical formula	$C_{22}H_{18}N_4$	$C_{22}H_{17}BrN_4$	$C_{30}H_{42}Cl_2N_4O_4RuS_2$	$C_{51.6}H_{55.2}Br_2Cl_2N_8O_4RuS$
fw	338.40	417.31	758.77	1215.29
space group	*Pbca*	$P2_1/c$	$P2_1/c$	$P\bar{1}$
a, Å	8.919(2)	11.0629(5)	15.366(3)	12.4094(3)
b, Å	19.849(4)	19.5840(9)	7.5306(2)	12.8933(3)
c, Å	20.229(46)	8.6930(5)	29.650(3)	18.5633(5)
α, deg				106.807(2)
β, deg		94.466(3)	104.11(3)	92.525(2)
γ, deg				108.003(2)
V, Å^3	3581.2(13)	1877.67(16)	3327.3(12)	2674.82(12)
Z	8	4	4	2
d_{calcd}, g cm^{-3}	1.255	1.476	1.515	1.509
μ, cm^{-1}	0.77	22.03	7.98	19.77
T, K	120	100	100	100
R1[a]	0.0419	0.0318	0.0347	0.0454
wR2[b]	0.1118	0.0807	0.0795	0.1389

[a] $R1 = \sum||F_o| - |F_c||/\sum|F_o|$. [b] $wR2 = \{\sum[w(F_o^2 - F_c^2)^2]/\sum[w(F_o^2)^2]\}^{1/2}$.

implemented in the *Gaussian 03*[41] program package. The basis set used was 6-311+G(d,p). The optimized bond lengths are in good agreement with experimental data, with an average deviation of $\pm 7.7 \times 10^{-3}$ Å. The united atom topological model optimized for HF/6-31G(d) calculations (UAHF) set of radii and default *Gaussian* methanol parameters were used in the polarizable continuum model (PCM)[42] calculations.

Cell Lines and Culture Conditions. A549 cells (non-small cell lung carcinoma) and SW480 cells (adenocarcinoma of the colon) were provided by Brigitte Marian, Institute of Cancer Research, Medical University of Vienna, Austria. CH1 cells originated from an ascites sample of a patient with a papillary cystadenocarcinoma of the ovary and were provided by Lloyd R. Kelland, CRC Centre for Cancer Therapeutics, Institute of Cancer Research, Sutton, U.K. The cells were grown in 75 cm^2 culture flasks (Iwaki) as adherent monolayer cultures in complete culture medium, i.e., Minimal Essential Medium, supplemented with 1 mM sodium pyruvate, 4 mM L-glutamine, 1% nonessential amino acids (100×) (all purchased from Sigma-Aldrich), and 10% heat-inactivated fetal bovine serum (purchased from Invitrogen). Cultures were maintained at 37 °C in a humidified atmosphere containing 5% CO_2.

Cytotoxicity Tests in Cancer Cell Lines. Cytotoxicity was determined by means of a colorimetric microculture assay (MTT assay, MTT = 3-(4,5-dimethyl-2-thiazolyl)-2,5-diphenyl-2*H*-tetrazolium bromide). For this purpose, A549, CH1, and SW480 cells were harvested from culture flasks by trypsinization and seeded into 96-well microculture plates (Iwaki). The following cell densities were chosen to ensure exponential growth throughout drug exposure: 4×10^3 cells/well for A549, 1.5×10^3 cells/well for CH1, and 2.5×10^3 cells/well for SW480 cells. After a 24 h preincubation period, cells were exposed to solutions of the test compounds in 200 μL/well complete culture medium for 96 h. For this purpose, the compounds were dissolved in DMSO and then serially diluted in complete culture medium such that the maximum effective DMSO content did not exceed 0.5%. At the end of the exposure, drug solutions were replaced by 100 μL/well RPMI1640 culture medium (supplemented with 10% heat-inactivated fetal bovine serum) plus a 20 μL/well MTT solution in phosphate-buffered saline (5 mg/mL). After incubation for 4 h, the medium/MTT mixtures were removed, and the formazan crystals formed by the mitochondrial dehydrogenase activity of vital cells were dissolved in 150 μL of DMSO per well. Optical densities at 550 nm were measured with a microplate reader (Tecan Spectra Classic), using a reference wavelength of 690 nm to correct for unspecific absorption. The quantity of vital cells was expressed in terms of T/C values by comparison to untreated control microcultures, and IC_{50} values were calculated from concentration−effect curves by interpolation. The evaluation is based on means from at least three independent experiments, each comprising six microcultures per concentration level.

Changes in DNA Secondary Structure. For all examinations, DMSO solutions of **2a** and **2b** were prepared, diluted with doubly distilled water to a final DMSO concentration of 6%, and stored immediately at −20 °C. Plasmid pTZ18u (2860 bp) was obtained from Biorad. The plasmid was transformed in DH5α cells, isolated, purified according to standard procedures, and dissolved in TE buffer.

Plasmid pTZ18u in the measure of 1 μg and increasing amounts (200, 400, 600, 800, and 1000 μM) of either compound **2a** or **2b** were incubated for 6 h in 10 mM $NaClO_4$ at 37 °C in a final volume of 40 μL. For detection of the changes in the DNA secondary structure, 20 μL of each reaction mixture was withdrawn and mixed with 5 μL of "blue juice" sample buffer (final: 2.5% glycerol, 0.5% SDS, 10 mM EDTA, 0.025% bromphenol blue, and 0.025% xylene cyanol). The second set of 20 μL samples was used for a duplicate experiment. The reaction products were separated immediately in a 1% agarose gel in 1XTBE buffer at 3 V/cm. The gel was stained with 0.2 μg/mL EtBr in 1XTBE, illuminated by UV light, and photographed using a gel documentation system from Vilber Lourmat (Torcy Z.I., Sud, France). To exclude a possible impact

(41) Frisch, M. J.; Trucks, G. W.; Schlegel, H. B.; Scuseria, G. E.; Robb, M. A.; Cheeseman, J. R.; Montgomery, J. A., Jr.; Vreven, T.; Kudin, K. N.; Burant, J. C.; Millam, J. M.; Iyengar, S. S.; Tomasi, J.; Barone, V.; Mennucci, B.; Cossi, M.; Scalmani, G.; Rega, N.; Petersson, G. A.; Nakatsuji, H.; Hada, M.; Ehara, M.; Toyota, K.; Fukuda, R.; Hasegawa, J.; Ishida, M.; Nakajima, T.; Honda, Y.; Kitao, O.; Nakai, H.; Klene, M.; Li, X.; Knox, J. E.; Hratchian, H. P.; Cross, J. B.; Bakken, V.; Adamo, C.; Jaramillo, J.; Gomperts, R.; Stratmann, R. E.; Yazyev, O.; Austin, A. J.; Cammi, R.; Pomelli, C.; Ochterski, J. W.; Ayala, P. Y.; Morokuma, K.; Voth, G. A.; Salvador, P.; Dannenberg, J. J.; Zakrzewski, V. G.; Dapprich, S.; Daniels, A. D.; Strain, M. C.; Farkas, O.; Malick, D. K.; Rabuck, A. D.; Raghavachari, K.; Foresman, J. B.; Ortiz, J. V.; Cui, Q.; Baboul, A. G.; Clifford, S.; Cioslowski, J.; Stefanov, B. B.; Liu, G.; Liashenko, A.; Piskorz, P.; Komaromi, I.; Martin, R. L.; Fox, D. J.; Keith, T.; Al-Laham, M. A.; Peng, C. Y.; Nanayakkara, A.; Challacombe, M.; Gill, P. M. W.; Johnson, B.; Chen, W.; Wong, M. W.; Gonzalez, C.; Pople, J. A. *Gaussian 03*, revision D.01; Gaussian, Inc.: Wallingford, CT, 2004.
(42) Miertus, S.; Scrocco, E.; Tomasi, J. *Chem. Phys.* **1981**, *55*, 117−129.

of DMSO on DNA, a control according to the described procedure was performed with DMSO alone at the corresponding concentrations. No effect whatsoever was observed.

Results and Discussion

Synthesis and Characterization of Ligands and Metal Complexes. A mild conversion of the thiolactam into the amidine functional group has been reported to proceed in the presence of mercury chloride, which favors the completion of the reaction by precipitation of mercury sulfide.[43−46] Another common approach to conversion consists of methylation of the thiolactam with methyl iodide and subsequent reaction of the formed methyl thioimidate with an amine.[47,48] Only a few syntheses were reported to proceed without the addition of a mercury salt or a methylating agent.[49,50] We performed the reaction of 7,12-dihydroindolo[3,2-*d*][1]-benzazepin-6(5*H*)-thione and 9-bromo-7,12-dihydroindolo-[3,2-*d*][1]benzazepin-6(5*H*)-thione with α-picolylamine taken in excess in refluxed dry THF and isolated the two amidines $\mathbf{L^1}$ and $\mathbf{L^2}$ (Scheme 1). This approach permitted the isolation of paullone-derived ligands in only one step without any additional reagent and in excellent yield (90 and 95% for $\mathbf{L^1}$ and $\mathbf{L^2}$, correspondingly) and purity. As the primary amine for binding to the paullone scaffold, we chose α-picolylamine, since a literature survey on the coordination chemistry of ruthenium showed that it is a convenient ligand for binding to ruthenium species and for stabilizing the formal oxidation state of 2+.[51−54] The complex *cis*-[$RuCl_2(DMSO)_4$] reacts with $\mathbf{L^1}$ and $\mathbf{L^2}$ in a 1:1 molar ratio in dry ethanol at 50 °C, affording the complexes *trans*-[$Ru^{II}Cl_2(DMSO)_2\mathbf{L^1}$] (**1a**) and *trans*-[$Ru^{II}Cl_2(DMSO)_2\mathbf{L^2}$] (**1b**) in 26 and 30% yield, respectively. The reaction carried out from the same starting compounds in a 1:2 molar ratio at 75 °C led to the formation of [$Ru^{II}Cl(DMSO)(\mathbf{L^1})_2$]Cl (**2a**) and [$Ru^{II}$-$Cl(DMSO)(\mathbf{L^2})_2$]Cl (**2b**) in 16 and 23% yield, correspondingly.

Differing only in the substituent at position 9 of the paullone scaffold (X = H or Br), both $\mathbf{L^1}$ and $\mathbf{L^2}$ and their complexes with 1:1 (**1a** and **1b**) and 1:2 metal-to-ligand stoichiometries (**2a** and **2b**) reveal similar spectroscopic properties.

The vibrational spectra of the two ligands display two broad bands of N−H groups at about 3400 and 3200 cm^{-1} and those of the aromatic C−H groups at 3050 cm^{-1}. At 1610 cm^{-1}, $\mathbf{L^1}$ and $\mathbf{L^2}$ show a strong and sharp C═N vibration, followed by a number of bands with decreasing intensity until 1150 cm^{-1}, forming a sawlike structure. Lines at about 750 cm^{-1} with intensities decreasing in the order $\mathbf{L^1}$, $\mathbf{L^2}$ > **1a**, **1b** > **2a**, **2b** can be ascribed to out-of-plane bending vibrations of the ortho-substituted benzene rings. Compared to the free ligands, the vibrational spectra of the complexes display similar N−H and C−H vibration bands, and the C═N vibration is blue-shifted to 1626 (**1b**, **2a**) or 1627 cm^{-1} (**1a**, **2b**). For all complexes, the bands between 1626 or 1627 and 1150 cm^{-1} are much weaker. In addition, absorption bands attributed to ν_{SO} at 1100−1050 cm^{-1}, ν_{RuS} at 426−430 cm^{-1}, and ν_{CSO} at 395−400 cm^{-1} (bending vibration) are present. These bands along with those ascribed to out-of-plane bending vibrations of the ortho-substituted benzene rings are markedly weaker for complexes **2a** and **2b**.

Electronic absorption spectra of all compounds show broad bands, some of them with associated shoulders. The maxima all lie in the three regions ranging from 229 to 237, 258 to 262, and 300 to 319 nm, $\mathbf{L^1}$ being the only exception with a fourth maximum at 268 nm, where only a shoulder is found for the other compounds. For the complexes **2a** and **2b**, two absorbance bands in the regions from 229 to 237 and from 300 to 319 nm are observed. Electronic absorption spectra of all compounds are very similar, and those of **2a** and **2b** possess larger extinction coefficients than those of **1a** and **1b**. All this indicates that the electronic absorptions are due to $\pi \rightarrow \pi^*$ transitions within the ligands. The Ru^{II}−Cl bond was expected to be labile, so the chloro ligand will be first substituted by the water ligand, which will be subsequently replaced by the nucleotides of DNA. However, electronic absorption spectra measured in methanol containing 10% water and in DMSO solutions diluted with water to a DMSO content of 4% showed only slight changes after 3 days, indicating minor hydrolysis of the Ru−Cl bond (Supporting Information, Figures S5 and S6).

The positive ion ESI mass spectra show the presence of peaks at *m*/*z* 339 and 419 attributable to [$\mathbf{L^1}$ + H]$^+$ and [$\mathbf{L^2}$ + H]$^+$, whereas those recorded in negative mode display peaks at *m*/*z* 337 and 417 assignable to [$\mathbf{L^1}$ − H]$^-$ and [$\mathbf{L^2}$ − H]$^-$. **1a** and **1b** display adduct formation with sodium and chloride ions detected in positive mode as [**1a** + Na]$^+$ and [**1b** + Na]$^+$ with peaks at *m*/*z* 691 and 769 and in negative mode as [**1a** + Cl]$^-$ and [**1b** + Cl]$^-$ at *m*/*z* 703 and 781, respectively. These complexes also show signals in negative mode at *m*/*z* 625 and 667 attributed to [**1a** − DMSO + Cl]$^-$ and [**1b** − DMSO − H]$^-$, respectively. For **2a** and **2b**, the complex cations [$Ru^{II}Cl(DMSO)(\mathbf{L^1})_2$]$^+$ and [$Ru^{II}Cl(DMSO)(\mathbf{L^2})_2$]$^+$ display peaks at *m*/*z* 891 and 1049, correspondingly. Strong peaks at *m*/*z* 813 and 971 were attributed to [$Ru^{II}Cl(\mathbf{L^1})_2$]$^+$ and [$Ru^{II}Cl(\mathbf{L^2})_2$]$^+$ ions.

(43) Eifler-Lima, V. L.; Uriac, P.; Huet, J.; Jenkins, T. C.; Thurston, D. E. *Bioorg. Med. Chem. Lett.* **1995**, *5*, 3003−3006.
(44) Bock, M. G.; DiPardo, R. M.; Evans, B. E.; Rittle, K. E.; Freidinger, R. M.; Chang, R. S.; Lotti, V. J. *J. Med. Chem.* **1988**, *31*, 264−268.
(45) Foloppe, M. P.; Rault, S.; Robba, M. *Tetrahedron Lett.* **1992**, *33*, 2803−2804.
(46) Delcros, J.-G.; Tomasi, S.; Duhieu, S.; Foucault, M.; Martin, B.; Le Roch, M.; Eifler-Lima, V.; Renault, J.; Uriac, P. *J. Med. Chem.* **2006**, *49*, 232−245.
(47) Kunick, C.; Link, A. *J. Heterocycl. Chem.* **1995**, *32*, 803−805.
(48) Wendelin, W.; Keimelmayr, H.; Huber, M. *Sci. Pharm.* **1989**, *57*, 27−38.
(49) Chauhan, P. M. S.; Martins, C. J. A.; Horwell, D. C. *Bioorg. Med. Chem.* **2005**, *13*, 3513−3518.
(50) Thurkauf, A.; Chen, X.; Zhang, S.; Gao, Y.; Kieltyka, A., Wasley, J. W. F.; Brodbeck, R.; Greenlee, W.; Ganguly, A.; Zhao, H. *Bioorg. Med. Chem. Lett.* **2003**, *13*, 2921−2924.
(51) Chang, J.; Plummer, S.; Berman, E. S. F.; Striplin, D.; Blauch, D. *Inorg. Chem.* **2004**, *43*, 1735−1742.
(52) Baratta, W.; Herdtweck, E.; Siega, K.; Toniutti, M.; Rigo, P. *Organometallics* **2005**, *24*, 1660−1669.
(53) Abdur-Rashid, K.; Abbel, R.; Hadzovic, A.; Lough, A. J.; Morris, R. H. *Inorg. Chem.* **2005**, *44*, 2483−2492.
(54) Ohkuma, T.; Sandoval, C. A.; Srinivasan, R.; Lin, Q.; Wei, Y.; Muòiz, Noyori, R. *J. Am. Chem. Soc.* **2005**, *127*, 8288−8289.

Conductivity measurements of **2b** in methanolic solution indicate a 1:1 electrolyte (1 mM, 66.7 μS/cm).[55] It should be noted that the formation of an aqua complex from **2b** with methanol residual water would result in a 2:1 electrolyte with a higher value of conductivity. No evidence of a hydroxo complex was found in mass spectra.

Remarkably, all compounds were found to be electrochemically silent in the range between −1.5 and +1.0 V vs NHE.

Crystal Structures. The formation of an amidine bond from a thiolactam and picolylamine has been corroborated by X-ray diffraction studies of paullone species $\mathbf{L^1}$ and $\mathbf{L^2}$, the results of which are shown in Supporting Information, Figures S1 and S2, respectively. The distribution of electron density over the azepine ring fragment involving the nitrogen atom N2 indicates the predominant double-bond character of the C12−N2 bond at 1.2968(13) Å ($\mathbf{L^1}$) and 1.298(2) Å ($\mathbf{L^2}$) compared with N2−C11 at 1.4043(13) Å ($\mathbf{L^1}$) and 1.405(2) Å ($\mathbf{L^2}$). A significant lengthening of the bond C12−N3 compared with C12−N2 in both compounds is also observed (see captions to Supporting Information, Figures S1 and S2). A salient structural feature of both $\mathbf{L^1}$ and $\mathbf{L^2}$ is the folded conformation of the seven-membered azepine ring, due to the presence of the methylene group carbon atom, which is solely sp^3-hybridized. This atom interrupts the conjugation of the whole π system, and the molecules as a whole are nonplanar. Restricted rotation around the phenyl−indole axis (C5−C6) in both compounds enables ring inversion. The dihedral angle between the phenyl and indole rings can be characterized by the torsion angle of $\Theta_{N1-C5-C6-C7}$, which is +27.58(15)° and −31.0(2)° in $\mathbf{L^1}$ and $\mathbf{L^2}$, respectively. The presence of another methylene group carbon atom in the picolylamine moiety makes it rather flexible, enabling rotation of the pyridine ring around the C13−C14 bond. Solid-state rotation of the pyridine ring is impeded by the formation of two strong symmetry-related intermolecular hydrogen bonds of the type N4···H−N3 (Supporting Information, Figure S3). Intermolecular hydrogen bonding is also observed between the azepine ring nitrogen atom N2 acting as proton acceptor and the indole nitrogen atom N1 acting as proton donor (Supporting Information, Figure S4).

The molecular structure of *trans*-[$Ru^{II}Cl_2(DMSO)_2(\mathbf{L^1})$] is shown in Figure 1. The coordination polyhedron of ruthenium(II) in **1a**·2EtOH approaches an octahedron. The organic ligand is coordinated to ruthenium in the equatorial plane via the picolylamine moiety, with interatomic distances Ru1−N3 at 2.122(2) Å and Ru1−N4 at 2.138(2) Å. These bond lengths are significantly shorter than those found in $RuHCl(PPh_3)_2$(ampy) at 2.163(2) and 2.171(2) Å, respectively[53] and comparable with those observed in *cis*-[$RuCl_2$-{$Ph_2P(CH_2)_4PPh_2$}(ampy)],[52] where ampy = α-picolylamine. The torsion angle of $\Theta_{N3-C13-C14-N4}$ at −20.4(3)° differs significantly from that found in $\mathbf{L^1}$ at 42.72(13)° but is far from approaching the 0° value expected for cis-equatorial binding. The other two equatorial places are occupied by DMSO molecules bound to Ru via S. The Ru1−S1 and

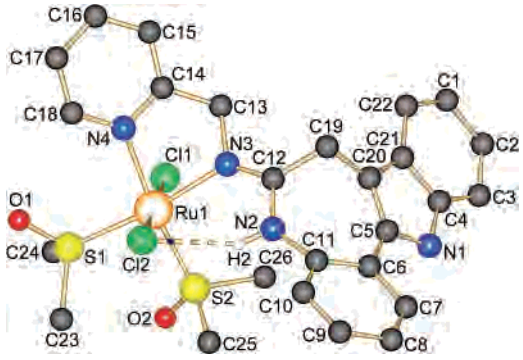

Figure 1. *SCHAKAL* view of the molecular structure of **1a** with the atom numbering scheme. All H atoms (with the exception of H2) were omitted for clarity. Selected bond lengths (Å) and bond angles and torsion angles (deg): Ru1−Cl1 2.4014(8), Ru1−Cl1 2.4261(8), Ru1−S1 2.2811(8), Ru1−S2 2.2572(9), Ru1−N3 2.122(2), Ru1−N4 2.138(2), S1−O1 1.494(2), S2−O2 1.484(2), C4−N1 1.370(4), N1−C5 1.387(4), C5−C6 1.455(4), C6−C11 1.406(4), C11−N2 1.405(4), N2−C12 1.366(3), C12−N3 1.298(4), C12−C19 1.503(4), C19−C20 1.499(4), C20−C5 1.369(4), C4−N1−C5 108.6(2), C11−N2−C12 130.7(2), N2−C12−N3 116.5(2), N3−C12−C19 126.7(3), C12−C19−C20 108.8(2), $\Theta_{N3-C13-C14-N4}$ −20.4(3), $\Theta_{N2-C12-C19-C20}$ 67.0(3), $\Theta_{N1-C5-C6-C7}$ 22.4(4). Intramolecular hydrogen bonding N2−H2···Cl2: N2−H2, 0.880 Å, H2···Cl2, 2.925 Å, N2···Cl2 3.197 Å; ∠N2H2Cl2, 152.75°.

Ru1−S2 bond lengths at 2.2811(8) and 2.2472(9) Å are well comparable with those found in other Ru−DMSO complexes.[56] The S1−O1 and S2−O2 interatomic distances at 1.494(2) and 1.484(2) Å are similar to that in the uncoordinated DMSO molecule at 1.492(1) Å.[57] The two axial chloro ligands Cl1 and Cl2 are at 2.4014(8) and 2.4261(8) Å bonding distances from Ru1, these values being normal for Ru−Cl bonds.[56,58,59] As in the metal-free ligand $\mathbf{L^1}$ (Supporting Information, Figure S1), the azepine ring in the ruthenium-bound $\mathbf{L^1}$ is folded. The torsion angle of $\Theta_{N1-C5-C6-C7}$ at 22.4(4)° is comparable but smaller than that in $\mathbf{L^1}$ (27.58(15)°). $\mathbf{L^1}$ in *trans*-[$Ru^{II}Cl_2(DMSO)_2(\mathbf{L^1})$]·2EtOH acts as a neutral ligand and is stabilized in a different tautomeric form compared with that in the metal-free one. Now, the hydrogen atom is attached to N2 and the N2−C12 bond length at 1.366(3) Å is significantly longer than that of C12−N3 at 1.298(4) Å, the latter possessing a pronounced double-bond character. Intramolecular hydrogen bonding is observed between Cl2 and H2, which "freezes" the exocyclic double bond in E configuration. The ethanol molecules partake in intermolecular hydrogen-bonding interactions, stabilizing the crystal lattice.

The molecular structure of the cation [$Ru^{II}Cl(DMSO)$-$(\mathbf{L^2})_2$]$^+$ in **2b**·2.8EtOH·0.2H_2O is shown in Figure 2. The coordination geometry of ruthenium(II) can be described as octahedral with bidentate ligand 1, one DMSO molecule, and the nitrogen atom N7 of ligand 2 in the equatorial plane and the chloro ligand and pyridine nitrogen N8 of the second paullone ligand occupying the axial positions. The torsion

(55) Geary, W. J. *Coord. Chem. Rev.* **1971**, *7*, 81−122.

(56) Reisner, E.; Arion, V. B.; Rufiñska, A.; Chiorescu, I.; Schmid, W. F.; Keppler, B. K. *Dalton Trans.* **2005**, 2355−2364.

(57) Calligaris, M.; Carugo, O. *Coord. Chem. Rev.* **1996**, 153, 83−154. Calligaris, M. *Coord. Chem. Rev.* **2004**, *248*, 351−375.

(58) Alessio, E.; Mestroni, G.; Nardin, G.; Attia, W. M.; Calligaris, M.; Sava, G.; Zorzet, S. *Inorg. Chem.* **1988**, *27*, 4099−4106.

(59) Jaswal, J. S.; Rettig, S. J.; James, B. R. *Can. J. Chem.* **1990**, *68*, 1808−1817.

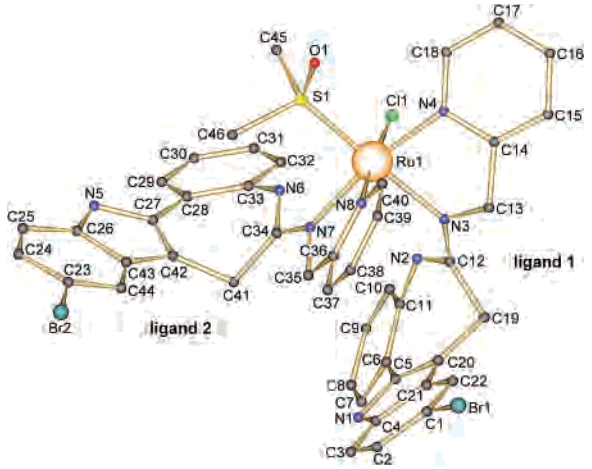

Figure 2. *SCHAKAL* view of the molecular structure of $[Ru^{II}Cl(DMSO)(\mathbf{L^2})_2]^+$, the cation of **2b**, with the atom numbering scheme. H atoms were omitted for clarity. Selected bond lengths (Å) and bond angles and torsion angles (deg): Ru1−Cl1 2.4597(10), Ru1−S1 2.2250(11), Ru1−N3 2.109(4), Ru1−N7 2.116(3), Ru1−N4 2.091(4), Ru1−N8 2.045(3), S1−O1 1.482(3), C4−N1 1.371(6), C26−N5 1.376(6), N1−C5 1.379(6), N5−C27 1.370(6), C5−C6 1.454(6), C27−C28 1.454(6), C6−C11 1.415(6), C28−C33 1.412(6), C11−N2 1.410(5), C33−N6 1.417(5), N2−C12 1.356(5), N6−C34 1.371(5), C12−N3 1.300(5), C34−N7 1.300(5), C12−C19 1.502(6), C34−C41 1.501(6), C19−C20 1.499(6), C41−C42 1.496(6), C20−C5 1.366(6), C42−C27 1.375(6), C4−N1−C5 108.7(4), C26−N5−C27 108.5(4), C11−N2−C12 129.4(4), C33−N6−C34 129.6(4), N2−C12−N3 117.3(4), N6−C34−N7 118.1(3), N3−C12−C19 124.8(4), N7−C34−C41 126.7(4), C12−C19−C20 102.5(3), C34−C41−C42 107.8(3), $\Theta_{N3-C13-C14-N4}$ = 34.9(5), $\Theta_{N7-C35-C36-N8}$ −9.8(5), $\Theta_{N2-C12-C19-C20}$ −76.0(4), $\Theta_{N6-C34-C41-C42}$ −65.3(4), $\Theta_{N1-C5-C6-C7}$ −32.4(6), $\Theta_{N5-C27-C28-C29}$ −30.4(7).

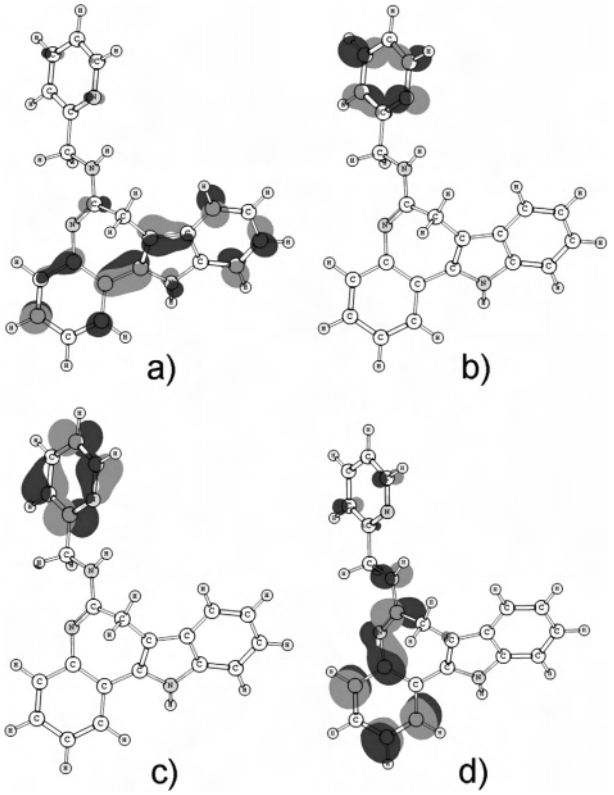

Figure 3. Four lowest unoccupied MOs of $\mathbf{L^1}$; each of these are potential acceptors for ligand-centered transitions. (a) LUMO orbital (−0.76 eV); (b) LUMO+1 (−0.64 eV); (c) LUMO+2 (−0.32 eV); (d) LUMO+3 (−0.08 eV).

angles of $\Theta_{N1-C5-C6-C7}$ and $\Theta_{N5-C27-C28-C29}$ at −32.4(6)° and −30.4(7)° are comparable with those observed in $\mathbf{L^2}$ (vide supra). Compared with those of **1a**·2EtOH, all Ru−N bonds are significantly shorter, possibly due to the loss of one trans-influencing and also sterically demanding DMSO ligand. The bonding distances of ruthenium to the amidine and pyridine nitrogen of ligand 1 are 2.109(4) and 2.091(4) Å, respectively, and 2.116(3) and 2.045(3) Å, respectively, for ligand 2. Hydrogen bonding is evident between the protonated azepine ring N atoms of both ligands and Cl1. As observed also in **1a**·2EtOH, this stabilizes the E configuration with the exocyclic double bond for both coordinated ligands. The corresponding bond lengths are given in the caption of Figure 2.

Calculated Gas-Phase Structure and Electronic Transitions of $\mathbf{L^1}$. The molecular geometry found in the crystal structure of $\mathbf{L^1}$ is a local minimum on the potential-energy surface. The gas-phase ground state was minimized and confirmed by vibrational analysis. In the absolute minimum structure, the atoms C12, N3, and C13 are in-plane with the pyridine moiety. This conformation is favorable for coordination to the transition metal and is actually found in the complexes.

The electronic absorption spectra of the ligands and the complexes display a number of ligand-centered $\pi \rightarrow \pi^*$ transitions. With the use of time-dependent density functional theory,[60] it is possible to model the excited states (nine singlet excited states were solved; see Figure 3) and to assign the transitions. PCM calculations (at the B3LYP/6-311+G(d,p) level) in methanol predict five transitions of reasonable intensity for $\mathbf{L^1}$ at approximately 324 nm (HOMO → LUMO; oscillator strength f = 0.32); 302 nm (a combination of HOMO−1 → LUMO and HOMO → LUMO+1; f = 0.12); 279 nm (a combination of HOMO−2 → LUMO and HOMO → LUMO+3; f = 0.11); 265 nm (HOMO−1 → LUMO+2; f = 0.12); and 258 nm (HOMO−1 → LUMO+3; f = 0.33).

^{1}H and ^{13}C NMR Spectra. In the ^{1}H NMR spectra of the free ligands $\mathbf{L^1}$ and $\mathbf{L^2}$, the resonance for the indole NH proton is found at ca. 11.5 ppm. Integration of the resonances between 8.5 and 7.0 ppm suggests that the second NH resonance overlaps with the aromatic proton signals. Indeed, a triplet at 7.8 ppm has the coupling constant of 5.3 Hz, like that of the methylene group at 4.5 ppm. This implies that the amidine double bond is located in the seven-membered azepine ring, which is consistent with the structures of $\mathbf{L^1}$ and $\mathbf{L^2}$ in the solid state, as determined by X-ray crystallography. The signal of the second methylene group is found at 3.4 ppm as a singlet, due to fast inversion of the azepine ring. The ^{13}C NMR spectra display aromatic and quaternary carbon resonances in the range of 160−109 ppm, whereas the two methylene carbon resonances are found at 47 and 29 ppm (Chart 2 and Figure 4).

By means of ^{1}H−^{1}H COSY, ^{1}H−^{1}H TOCSY, ^{1}H−^{13}C HMQC, ^{1}H−^{13}C HMBC, and NOE difference experiments, ^{1}H and ^{13}C resonances were assigned for compounds $\mathbf{L^1}$, $\mathbf{L^2}$, **1a**, **1b**, and **2b**. Because of several overlapping signals in

(60) Stratmann, R. E.; Scuseria, G. E.; Frisch, M. J. *J. Chem. Phys.* **1998**, *109*, 8218−8224.

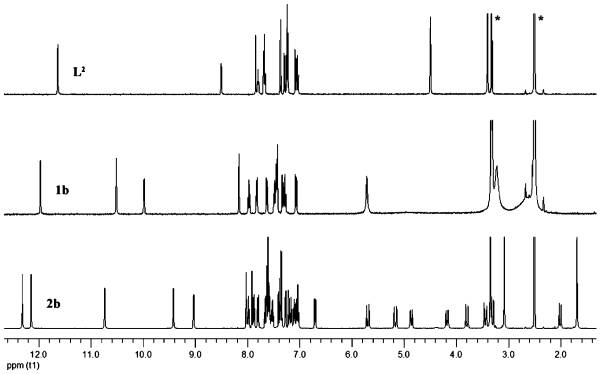

Figure 4. ^{1}H NMR spectra in DMSO-d_6 of $\mathbf{L^2}$ (upper trace), **1b** (middle trace), and **2b** (lower trace). Solvent signals are indicated by asterisks; details of the aromatic region (6.6−8.6 ppm) are depicted in Supporting Information, Figure S7.

Chart 2. NMR Numbering Scheme for $\mathbf{L^1}$, $\mathbf{L^2}$, **1a**, **1b**, **2a**, and **2b**

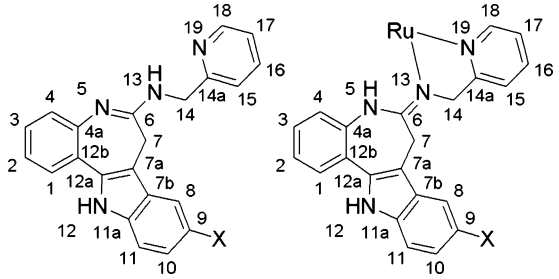

the aromatic region of its ^{1}H NMR spectrum, no two-dimensional spectra were recorded for compound **2a**. An overview, including all assigned ^{1}H, ^{13}C, and ^{15}N chemical shifts (obtained by ^{1}H−^{15}N HMQC), is presented in Supporting Information, Tables S1 and S2.

Coordination of $\mathbf{L^1}$ and $\mathbf{L^2}$ to ruthenium(II) results in a significant downfield shift for the resonances of those atoms in close proximity to the ruthenium center. In particular, the ^{1}H and ^{13}C resonances of C^{18}H of the pyridine ring are shifted in both **1a** and **1b** from 8.5 and 150 ppm to 10 and 155 ppm, respectively. The shift of the amidine NH proton resonance is even larger, going from 7.8 to 10.5 ppm, and the picolylamine methylene group displayed a singlet shifted from 4.5 to 5.7 ppm. The large ^{15}N shift observed for the protonated amidine N atom from 77 to 106 ppm is due to the rearrangement of the ligand tautomeric form, with an endocyclic double bond at the amidine unit switched to that with an exocyclic double bond. This structural feature is also in accordance with the X-ray diffraction studies. Obviously, in the case of an exocyclic double bond, the ligands are stabilized by the resulting dπ−pπ^*-back-bonding interactions between the ruthenium center and the N sp^2 atom. Upon coordination, the ^3J coupling constant of H^{18} increases from 4.7 to 5.4−5.6 Hz. Interestingly, in the ^{1}H NMR spectra of **1a** and **1b**, the resonances of the DMSO methyl groups and the picolylamine methylene group are very broad. The azepine methylene group at 5 ppm can hardly be distinguished from background (Figure 4). Also, the DMSO methyl groups did not show any signal in the ^{13}C NMR spectra. A possible reason for this behavior might be a hindered rotation of the DMSO ligands around the Ru−S bond.

Table 2. Cytotoxicity of **2a** and **2b** in Three Human Cancer Cell Lines

	IC$_{50}$ (μM)[a]		
compound	A549	CH1	SW480
2a ($\mathbf{L^1}$)	>23	2.5 ± 0.2	9.4 ± 0.4
2b ($\mathbf{L^2}$)	≫12.5	3.2 ± 0.2	>12.5

[a] 50% inhibitory concentrations in A549, CH1, and SW480 cells after exposure for 96 h in the MTT assay. Values are means ± standard deviations from at least three independent experiments.

^{1}H and ^{13}C NMR spectra of **2b** reveal two sets of signals for the paullone ligands, indicating C_1 symmetry for this complex in solution. Unlike the broad ^{1}H resonances from the DMSO methyl groups and the two methylene groups in complexes **1a** and **1b**, this complex displays sharp proton resonances, demonstrating that DMSO rotation is blocked. The four methylene groups of the complex are diastereotopic due to the relatively crowded coordination sphere of the ruthenium center displaying eight separated doublets in the range from 2.01 to 5.70 ppm. Although both paullone ligands have the same chemical structure, they become inequivalent upon binding to ruthenium. The ligand coordinating with its amidine nitrogen atom N^{13} trans to DMSO will be referred to as ligand 1 and the ligand coordinating with its pyridine nitrogen N$^{19'}$ trans to the chloro ligand as ligand 2. NMR shifts can be used to draw conclusions about the electron density distribution, thereby providing a deeper insight into the binding situation in this complex. Thus, the δ values for the amidine NH proton of both coordinated ligands differ by 1.32 ppm, namely, 10.74 ppm for ligand 1 and 9.42 ppm for ligand 2. An even more pronounced difference of 1.77 ppm is detected for H^{18} next to the coordinating pyridine nitrogen. The resonance of this proton is found at 7.27 ppm for ligand 1 and at 9.04 ppm for ligand 2. These findings indicate that the electron density in ligand 1 is mainly withdrawn from its amidine part, whereas in ligand 2, the electron density is withdrawn from the pyridine moiety, i.e., from the nitrogen atoms featuring π-acceptor ligands in trans position. This finding is also reflected in the corresponding bond lengths of **2b**·2.8EtOH·0.2H$_2$O in the solid state (vide supra).

Cytotoxicity. The compounds **2a** and **2b** were tested for their antiproliferative activity in three human cancer cell lines by means of the colorimetric MTT assay. To avoid precipitation of the compounds upon dilution of DMSO stocks in the buffered culture medium (pH 7.4), the maximum effective concentrations applied had to be chosen as 25 μM in the case of **2a** and 12.5 μM in the case of **2b**. A comparison with the metal-free ligands $\mathbf{L^1}$ and $\mathbf{L^2}$ and with complexes **1a** and **1b** could not be drawn because of their insufficient solubility in the cell culture medium. The IC$_{50}$ values of compounds **2a** and **2b** are listed in Table 2, and complete concentration−effect curves are depicted in Figure 5.

Though the differences between the two compounds are not very pronounced, the complex **2a** tends to be slightly more cytotoxic than **2b** in all three cell lines, suggesting that a bromo substituent in position 9 is not advantageous. This structure−activity relationship is opposite to that reported by Kunick et al. for kenpaullone and 9-H paullone,[18] which

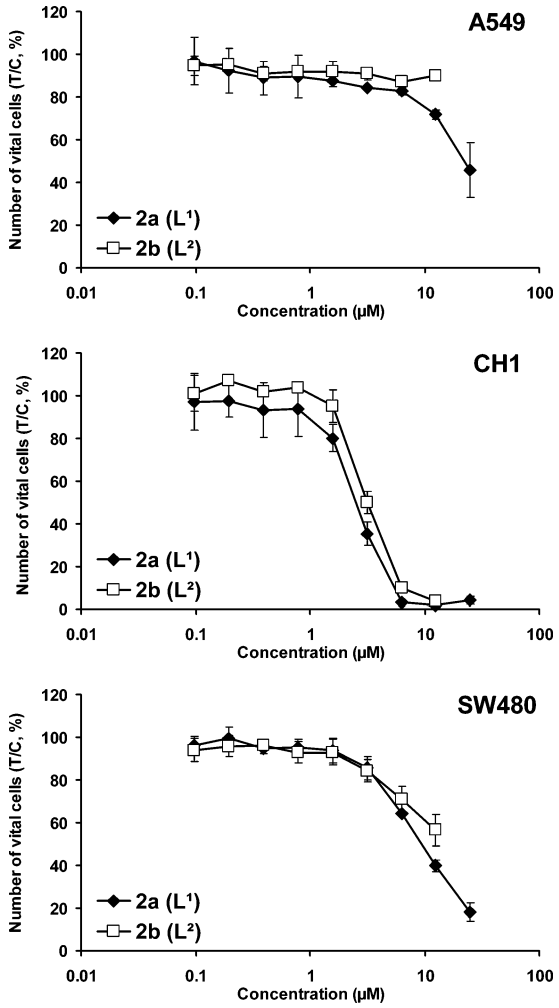

Figure 5. Concentration−effect curves of the ruthenium(II) complexes **2a** and **2b** in A549, CH1, and SW480 cells, obtained upon exposure for 96 h in the MTT assay. Values are means ± standard deviations of at least three independent experiments.

are the precursors for ligands $\mathbf{L^2}$ and $\mathbf{L^1}$, respectively. The IC_{50} values range from 2.5 to >23 μM in the case of complex **2a**, whereas the IC_{50} values could not be determined for **2b** in two of the three cell lines.

Stoichiometric mixtures of **2b** and 5′-GMP were analyzed by UV−vis and ^{1}H and ^{31}P NMR studies and showed no binding of the complex to this model DNA nucleotide within 72 h at 37 °C. As a consequence, we supposed that the antiproliferative activity of **2a** and **2b** might be caused by an intercalative or another noncovalent interaction with DNA or interaction with other cellular targets, e.g., CDKs. The species responsible for cytotoxicity appears to be the intact monocation. Examples of cationic complexes stable to hydrolysis but exhibiting cytotoxic activity have been documented in the literature.[61,62]

Changes in DNA Secondary Structure. To examine the alterations in DNA secondary structure, mass titration studies of compounds **2a** and **2b** with plasmid DNA were performed. Changes of DNA secondary structures can easily be monitored by evaluating the electrophoretic migration pattern of a circular dsDNA plasmid in neutral agarose gels. Adducts that untwist dsDNA effect a slower migration of the negatively "supercoiled" (sc) form of the plasmid as a result of partial relief of the torsional stress and consequent relaxing of the compact sc form; a faster migration of the nicked, "open circular" (oc) form of a plasmid, on the other hand, is consistent with adducts that apparently "condense" dsDNA and obviously overcome the effects of the increased molecular weight and positive charges.[63] Conversely, analyzing the DNA secondary structure may provide valuable clues about the kinds of DNA adducts; for example, untwisting of dsDNA may be effected by monofunctional or intercalating adducts, whereas the DNA might be compacted by multiple offset bends caused by bifunctional adducts.[64,65]

Figure 6 shows the agarose gels, in which increasing amounts of the ruthenium complexes **2a** and **2b** have been bound to plasmid pTZ18u. Both compounds showed a clear relaxation of the sc form of the plasmid, whereas the relaxation was slightly more pronounced in the presence of compound **2a** at equivalent concentrations. Although relaxation of the sc form is usually effected by (at least) monofunctional coordination of metal complexes and unwinding of dsDNA, in this case we cannot conclusively distinguish between monofunctional coordination and simple intercalation, which also effects unwinding. However, since no binding of **2a** and **2b** was detected toward the model nucleotide GMP, the detected untwisting could rather mirror intercalation of **2a** and **2b** into DNA. Moreover, fading of ethidium bromide staining of the plasmid with increasing amounts of compound, indicative of ethidium displacement or exclusion, also corroborates intercalation. Hence, several lines of evidence support an intercalative mode of interaction of the monocation with DNA.

Obviously, the mobility of the oc form of the plasmid was *decelerated* by **2a** and **2b**, which precludes a compaction of the DNA. Thus, the deceleration may signify that no stable bends or hinge joints were introduced into the DNA structure and that the slower migration may have been in fact due to increased molecular weight and positive charges introduced by **2a** and **2b**.

The slightly higher efficiency of **2a** to alter the DNA secondary structure compared with **2b** might be the cause of the slightly higher cytotoxic activity of **2a** in the examined cell lines, possibly due to the more efficient formation of cytotoxic DNA lesions. Due to the probable intercalative binding mode to DNA, we predict the compounds **2a** and

(61) Hotze, A. C. G.; Van der Geer, E. P. L.; Kooijman, H.; Spek, A. L.; Haasnoot, J. G.; Reedijk, J. *Eur. J. Inorg. Chem.* **2005**, *13*, 2648−2657.
(62) Barnard, P. J.; Baker, M. V.; Berners-Price, S. J.; Day, D. D. *J. Inorg. Biochem.* **2004**, *98*, 1642−1647.
(63) Cohen, G. L.; Bauer, W. R.; Barton, J. K.; Lippard, S. J. *Science* **1979**, *203*, 1014−1016.
(64) Lepre, C. A.; Lippard, S. J. Interaction of platinum antitumor compounds with DNA. In *Nucleic Acids and Molecular Biology*; Eckstein, F., Lilley, D. M. J., Eds.; Springer-Verlag: Berlin, Heidelberg, 1990; Vol. 4, pp 9−38.
(65) Keck, M. V.; Lippard, S. J. *J. Am. Chem. Soc.* **1992**, *114*, 3386−3390.

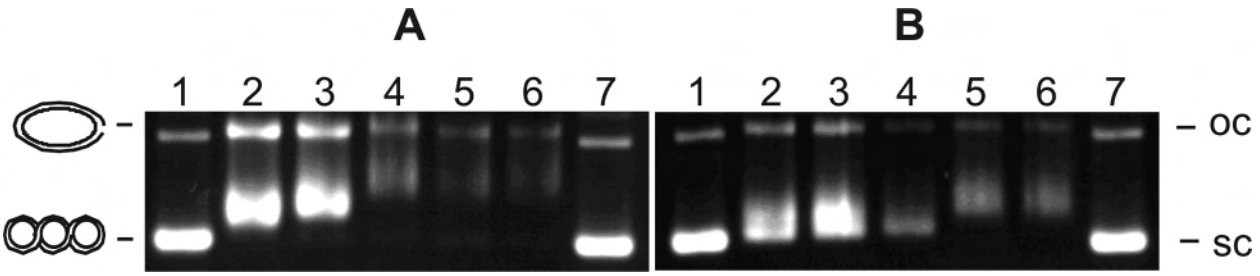

Figure 6. Interaction of increasing amounts of compounds **2a** (A) and **2b** (B) with plasmid pTZ18u for 6 h at 37 °C and electrophoretic separation in 1% agarose gel stained with EtBr. Lanes 2−6 (A, B): 200, 400, 600, 800, and 1000 μM. Lane 1: control DNA, not incubated. Lane 7: control DNA, incubated for 6 h.

2b to not display cross-resistance to other metal complexes, e.g., cisplatin, which functions by coordinative binding to DNA.

Final Remarks. Attachment of the α-picolylamine moiety to the paullone framework by chemical modification of the lactam unit made the paullone ruthenation possible. Complexes with 1:1 and 1:2 ruthenium-to-paullone ligand ratios have been isolated and fully characterized. In these complexes, the metal ion is chelated by one and two bidentate ligands, respectively. In contrast to the free ligands, which were found to exist as tautomers with an endocyclic azepine ring double bond both in the solid state and in solution, ruthenation stabilizes the tautomeric form with an exocyclic double bond by π-back-bonding interactions. The exocyclic double bond is found in an E configuration of the ligands due to hydrogen bonding between the protonated amidine nitrogen atom and a chloro ligand in all complexes. The ruthenium complexes presented herein are only the second example of metal-based paullone derivatives. Work is in progress to gain more insight into the factors that determine the biological activity of metalated paullones.

Acknowledgment. We thank Prof. G. Giester for the collection of the X-ray data set of $\mathbf{L^1}$. S.Z.-S. and H.Z. express their gratitude to Prof. Dieter Oesterhelt, Director of the Max-Planck-Institute of Biochemistry, Martinsried, Department of Membrane Biochemistry, for continuous and generous support.

Supporting Information Available: Molecular structures of $\mathbf{L^1}$ and $\mathbf{L^2}$; intermolecular hydrogen bonding in the crystal structure of $\mathbf{L^1}$; time-dependent UV−vis spectra of **1b** and **2b** in MeOH/H_2O = 90:10; details of ^{1}H NMR spectra of $\mathbf{L^2}$, **1b**, and **2b**, 6.6−8.6 ppm; assigned NMR shifts of $\mathbf{L^1}$, $\mathbf{L^2}$, **1a**, **1b**, and **2b**; crystallographic data of $\mathbf{L^1}$, $\mathbf{L^2}$, **1a**·2EtOH, and **2b**·2.8EtOH·0.2H_2O in CIF format. This material is available free of charge via the Internet at http://pubs.acs.org.

IC070098J